Available online at www.sciencedirect.com
SCIENCE DIRECT®
Engineering Structures 26 (2004) 13–25
ENGINEERING STRUCTURES
www.elsevier.com/locate/engstruct

# Nonlinear finite element analysis of deep reinforced concrete coupling beams

Z.Z. Zhao [a], A.K.H. Kwan [b,*], X.G. He [c]

[a] Department of Civil Engineering, Tsinghua University, Beijing, China
[b] Department of Civil Engineering, The University of Hong Kong, Pokfulam Road, Hong Kong, China
[c] Institute of Building Research and Design, Tsinghua University, Beijing, China

Received 22 May 2003; received in revised form 11 August 2003; accepted 11 August 2003

**Abstract**

A finite element method for analysing the nonlinear behaviour of reinforced concrete structures that accounts for cracking and compression-softening of the concrete and dowel action and confining effect of the reinforcing bars has been developed by the second and third authors. It was applied in this project to study the load–deflection behaviour and failure characteristics of deep reinforced concrete coupling beams by analysing the models previously tested by the first and second authors and using it to conduct a parametric study on the effects of varying the shear reinforcement and restraining the axial elongation of the coupling beams. The analysis showed good agreement between the theoretical and experimental results and revealed that deep coupling beams behave quite differently from ordinary beams; after cracking, a deep coupling beam behaves more like a truss with a diagonal concrete strut which rotates and causes axial elongation. On the other hand, the parametric study revealed that although adding more shear reinforcement could suppress shear-tension failure, it would cause shear-sliding failure at the beam–wall joints and that although restraining the axial elongation could increase the shear capacity, it would at the end lead to a more brittle failure.


*Keywords:* Coupling beams; Shear walls; Concrete structures; Finite element analysis

## 1. Introduction

Shear walls are commonly used in tall concrete buildings to resist lateral loads. Due to the presence of regular door or window openings, a shear wall is often divided into smaller wall units coupled together by coupling beams. During a major earthquake, if the coupling beams were very strong, the wall units might fail due to the large axial forces and bending moments induced in them without prior yielding of the coupling beams. As the walls are taking vertical loads and are the major lateral loads resisting elements, any damage to the walls could endanger the safety of the building and render the repair after earthquake very difficult. On the other hand, if the coupling beams were not too strong, they would yield and dissipate the excessive vibration energy before the wall units yield thereby reducing the axial forces induced in the walls and protecting the walls from being damaged. Hence, the coupling beams should be designed to yield before the walls yield but then the coupling beams would be subjected to a certain ductility demand. In any case, the earthquake resistance of a coupled shear wall structure is highly dependent on the nonlinear behaviour, especially the strength and ductility, of the coupling beams.

Since the widths of door and window openings usually range from 1.0 to 1.5 m, most coupling beams are quite short and deep and have span/depth ratios of 2.0 or even lower. Being more like deep beams, coupling beams with span/depth ratios lower than 2.0 tend to fail in shear rather than in flexure. Extensive tests of coupling beam models and coupled shear wall models aiming to study the nonlinear behaviour and failure characteristics of deep reinforced concrete coupling beams [1–4] and to investigate the effects of the nonlinear behaviour of coupling beams on the structural performance of coupled shear wall structures [5,6] have been carried out. The

* Corresponding author. Tel.: +852-2859-2647; fax: +852-2559-5337.
*E-mail address:* khkwan@hku.hk (A.K.H. Kwan).

0141-0296/$ - see front matter © 2003 Elsevier Ltd. All rights reserved.
doi:10.1016/j.engstruct.2003.08.014

coupling beam tests revealed that deep coupling beams behave quite differently from ordinary beams in frame structures and that significant local deformation occurs at the beam–wall joints. On the other hand, the coupled shear wall tests revealed that both under-coupling, which leads to early yielding of the coupling beams and thus a high ductility demand, and over-coupling, which leads to failure of the coupled shear wall structure without prior yielding of the coupling beams, are undesirable.

Regarding theoretical studies, coupling beams have been treated as ordinary beams and coupled shear walls analysed by modelling the coupling beams either as an equivalent continuous shear medium [7,8] or as discrete beam elements with horizontal rigid arms incorporated to simulate the rigid portions of the beams within the walls [9,10]. The finite element method has also been applied to analyse coupled shear walls by modelling the walls, coupling beams and beam–wall joints with plane stress elements, beam elements with no rigid arms, and transition zone elements, respectively [11]. These studies were generally based on assumed elasto-plastic or nonlinear load–deflection behaviour of the coupling beams and aimed at evaluating the possible effects of the nonlinear behaviour of the coupling beams on the overall structural performance of the coupled shear wall structure. None of these studies were able to analyse the nonlinear behaviour of deep coupling beams, which generally have limited ductility and in reality do not behave like ordinary beams. That was the reason why in these studies, the beam elements modelling the coupling beams needed to be assumed to have certain nonlinear load–deflection behaviour, which was treated as input data rather than output result of the analysis.

There have been few theoretical studies on the failure behaviour of deep coupling beams. Subedi [12,13] has investigated the failure modes of deep coupling beams and proposed a mathematical model for representing the major shear failure mode—the diagonal splitting failure mode (this particular shear failure mode is referred to as the shear-tension failure mode in this paper). His investigations revealed that the failure behaviour of deep coupling beams actually differs quite significantly from the conventional double-curvature bending concept of ordinary beams subjected to vertical shear and contraflexural bending moments at the ends. His mathematical model would allow the ultimate capacities of coupling beams failing under the diagonal splitting mode to be predicted but would not produce any nonlinear load–deflection curves for evaluating the ductility of the coupling beams or analysing the overall structural performance of the coupled shear wall structure. In fact, there is still no theoretical method available for evaluating the nonlinear load–deflection behaviour of deep coupling beams.

Although before cracking, a deep coupling beam behaves like an ordinary beam subjected to flexure, after cracking, it behaves more like a truss with a diagonal concrete strut [1,2]. Hence, the assumption that plane sections remain plane after deformation is not applicable to a cracked coupling beam. To analyse the nonlinear load–deflection behaviour and failure characteristics of a coupling beam, which cracks quite extensively before failing, the coupling beam must not be modelled as an ordinary beam using any beam element. In fact, since the nonlinear behaviour of a coupling beam is highly dependent on the boundary conditions, the reinforcement layout, the crack pattern and the steel–concrete interaction at the cracks, it would seem that the only suitable method of analysis is to model the coupling beam itself by finite elements. Furthermore, as significant interaction between the coupling beam and the walls connected to the coupling beam occurs at the beam–wall joints and the local deformations of the wall panels near the beam–wall joints may have certain effects on the behaviour of the coupling beam, the wall panels in the vicinity of the beam–wall joints need to be included as integral parts of the coupling beam in the finite element analysis.

However, although the finite element method has been widely used for the analysis of reinforced concrete structures [14,15], very few, if any at all, detailed nonlinear analysis of reinforced concrete coupling beams using the finite element method has been attempted. In the research project reported herein, the nonlinear finite element method recently developed by the second and third authors [16,17] was employed to study the nonlinear load–deflection behaviour and failure characteristics of deep reinforced concrete coupling beams. It was first applied to analyse the four large-scale coupling beam models tested by the first and second authors [18] to verify its applicability to coupling beams and to study the fine details of the stress distribution/ redistribution in the concrete and the steel reinforcement, the local deformations at the beam–wall joints and the failure mechanisms, which might not have been fully revealed in the tests. After then, it was used to conduct a parametric study on the effects of adding more shear reinforcement and restraining the axial elongation of the coupling beams by analysing coupling beam models with different amounts of shear reinforcement added and with different boundary conditions imposed.

## 2. Model testing of coupling beams

### 2.1. Test method

Although extensive testing of coupling beam models has been performed, the boundary conditions that the rotations of the two ends of a coupling beam are equal and that local deformations occur at the beam–wall joints, which could have substantial influences on the behaviour of the coupling beam, had not been correctly simulated in most of the previous tests. To resolve the

problem, the first and second authors have developed a new method of testing coupling beams that ensures equal rotations at the ends of the coupling beam specimen by incorporating a rotation restraining mechanism in the test set-up and takes into account local deformations at the beam–wall joints by incorporating the wall panels connected to the coupling beam as integral parts of the coupling beam specimen [18]. Since the test method has been reported in an earlier paper, only an outline is presented herein.

The test set-up is shown in Fig. 1. As shown in the figure, the coupling beam specimen is erected with its longitudinal axis in the vertical direction. One end of the specimen is fixed to a rigid ground beam and the other end is connected at to a T-shaped steel-loading frame. Shear load is applied to the specimen through the loading frame by a servo-controlled hydraulic actuator, whose loading and support ends are pin-connected to the loading frame and a horizontal reaction frame respectively. The line of action of the applied load is aligned to pass through the centre of the specimen. A rotation restraining mechanism consisting of two parallelogram-shaped pin-jointed trusses is installed to ensure that the rotations of the two ends of the specimen are equal. There is no restraint on the deformation of the specimen if the two ends of the specimen are parallel (i.e. rotate by the same amount). But if the two ends of the specimen are not parallel (i.e. rotate by different amounts), the rotation restraining mechanism will force the two ends to remain parallel. Apart from restraining the end rotations to be equal, the mechanism will not impose any restraint on the axial elongation/shortening of the specimen. On the other hand, out-of-plane movements of the loading frame and the specimen are restrained by the provision of roller guides. Regarding the test procedure, the specimen is tested under load control before the main reinforcement starts to yield. After yielding of the main reinforcement, the control mode is changed to displacement control so that the post-peak behaviour of the specimen may be measured.

Using this newly developed test method, a number of large-scale coupling beam models have been tested monotonically [18] and cyclically [19]. In this theoretical study, only the four monotonically tested specimens are analysed.

### 2.2. Models tested

The four monotonically tested coupling beam specimens were named as MCB1, MCB2, MCB3 and MCB4, respectively. They were 1/2-scaled and have similar longitudinal reinforcement ratios and similar transverse reinforcement ratios but different span/depth ratios of 1.17, 1.40, 1.75 and 2.00, respectively. Fig. 2 shows the dimensions and details of one of the coupling beam

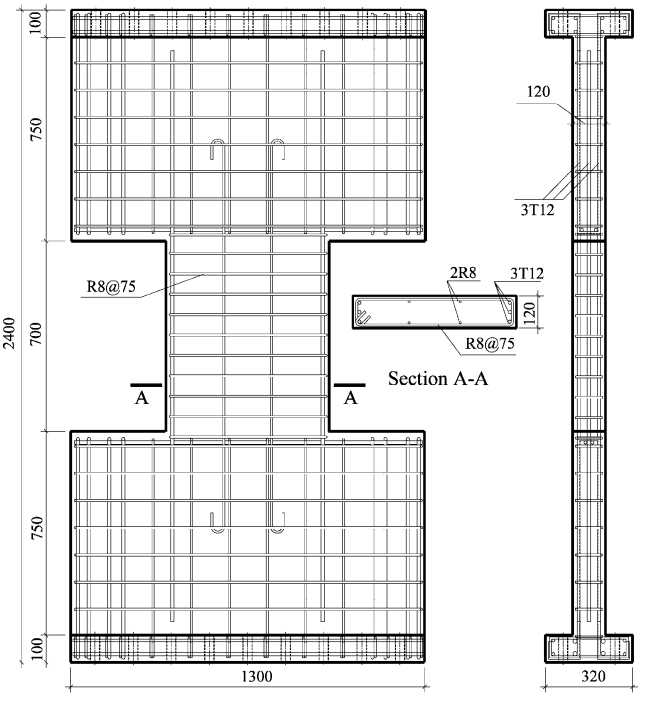


Fig. 2. Dimensions and details of MCB1.

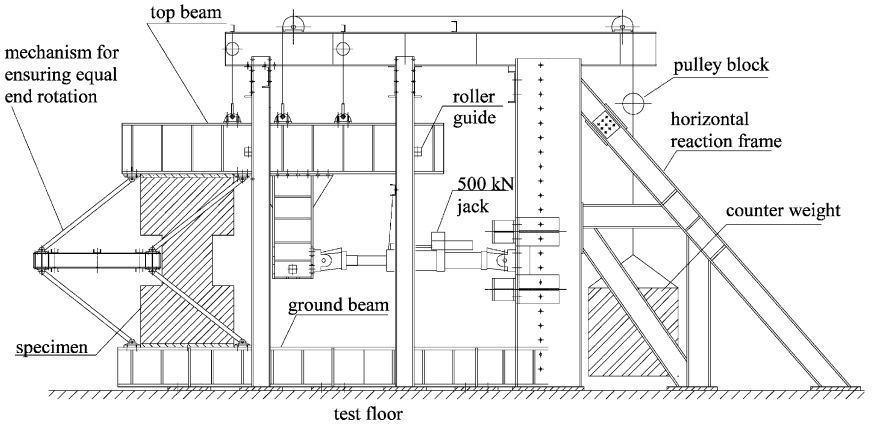


Fig. 1. Test set-up.

specimens tested. With the thickness and clear span of the specimens fixed at 120 and 700 mm, respectively, different span/depth ratios were obtained by varying the depth of the coupling beam. At each end of a coupling beam specimen, a rectangular end block (1300 × 750 mm) having the same thickness as the coupling beam and representing part of the wall connected to the coupling beam was cast integrally as part of the specimen. These end blocks were to allow for local deformations at the beam–wall joints.

Table 1 lists the structural parameters of the four specimens. In each specimen, equal amounts of top and bottom longitudinal reinforcement were provided throughout the length of the coupling beam. Additional longitudinal reinforcement was placed near mid-depth of the beam section. All longitudinal reinforcing bars in the coupling beam were provided with generous anchorage into the end blocks. Stirrups were provided in each coupling beam specimen as shear reinforcement. All specimens were cast of normal strength concrete with their planes lying horizontally. High-yield deformed bars (T12 and T8) were used as main longitudinal reinforcement whereas mild steel plain round bars (R8) were used for the additional longitudinal reinforcement and the stirrups. The detailed test results have been presented in Ref. [18].

## 3. Finite element analysis of coupling beams

### 3.1. Methodology

The finite element method developed by the second and third authors is used to analyse the coupling beam models. It has been successfully applied to study the effects of dowel action of reinforcing bars on the shear behaviour of deep beams [16] and the effects of concrete confinement on the behaviour of shear walls [17]. Since the details of the method have been presented elsewhere, only an outline is presented herein.

The concrete and the steel reinforcement inside are together modelled by a plane stress element, which is a four-noded isoparametric quadrilateral element with two extra non-conforming bending modes included to remove shear locking. A 2 × 2 grid of Gauss points is used in the numerical integration to obtain the element stiffness matrix. The constitutive matrix of the element consists of two parts, one contributed by the concrete and the other contributed by the steel reinforcement. For the concrete, the constitutive matrix is formed in the usual way taking into consideration the biaxial behaviour of the material. A smeared crack model is adopted. The concrete is assumed to be isotropic before cracking and orthotropic after cracking. Tension softening and compression softening are allowed for in the stress–strain relation. For the steel reinforcement, the constitutive matrix is formed by assuming that the reinforcing bars are perfectly bonded to the concrete and smeared, i.e. uniformly distributed, throughout the concrete element containing them. A tri-linear stress–strain relation with yielding and strain hardening incorporated is assumed for the reinforcing bars. Moreover, the stress transfer across cracks due to bond and dowel actions of reinforcing bars and the confinement effects of transverse reinforcement provided are also considered.

### 3.2. Analysis procedure

During the analysis, the loads are applied incrementally either directly in the form of prescribed loads or indirectly in the form of prescribed displacements at the loading points. At each load–displacement increment step, direct iteration using secant stiffness of the structure is employed so that the analysis may be extended into the post-peak range within which the tangent stiffness can become zero or negative. In this particular study, the loads are applied indirectly through prescribed displacements at the loading points for two reasons: first, the coupling beam models to be analysed were actually tested under displacement control when they failed; second, analysis with loads applied as prescribed displacements would allow the post-peak behaviour to be obtained.

Table 1
Structural parameters of the coupling beam specimens tested[a]

| Specimen | Span/depth ratio | Top and bottom longitudinal reinforcement (ratio) | Additional longitudinal reinforcement | Transverse reinforcement (ratio) |
|---|---|---|---|---|
| MCB1 | 1.17 | 3T12 (0.49%) | 4R8 | R8 @ 75 c/c (1.07%) |
| MCB2 | 1.40 | 2T12+T8 (0.49%) | 4R8 | R8 @ 75 c/c (1.07%) |
| MCB3 | 1.75 | 2T12 (0.50%) | 2R8 | R8 @ 75 c/c (1.07%) |
| MCB4 | 2.00 | T12+2T8 (0.56%) | 2R8 | R8 @ 75 c/c (1.07%) |

[a] T and R denote high-yield deformed bars and mild steel plain round bars. Equal amounts of longitudinal reinforcement were provided at the top and the bottom of the beam section. The additional longitudinal reinforcement was provided at mid-depth of the beam section.

Table 2
Properties of the steel reinforcing bars[a]

| Type | Area (mm$^2$) | $f_y$ (MPa) | $\varepsilon_y$ ($\mu\varepsilon$) | $f_{y1}$ (MPa) | $\varepsilon_{y1}$ ($\mu\varepsilon$) | $f_{y2}$ (MPa) | $\varepsilon_{y2}$ ($\mu\varepsilon$) | $E_s$ (GPa) |
|---|---|---|---|---|---|---|---|---|
| R8 | 48.1 | 346 | 1730 | 346 | 30,000 | 480 | 252,000 | 200 |
| T8 | 54.0 | 517 | 2585 | 517 | 28,000 | 717 | 173,000 | 200 |
| T12 | 111.6 | 525 | 2625 | 525 | 29,000 | 637 | 184,000 | 200 |

[a] $f_y$, $f_{y1}$ and $f_{y2}$ are the stresses at yield, at start of strain hardening and at ultimate state. $\varepsilon_y$, $\varepsilon_{y1}$ and $\varepsilon_{y2}$ are the strains at yield, at start of strain hardening and at ultimate state.

## 4. Numerical results

The above finite element method has been applied to analyse the four previously tested specimens, MCB1, MCB2, MCB3 and MCB4 to verify its applicability to deep coupling beams and to study the fine details of the nonlinear behaviour of deep coupling beams which might not have been revealed during the tests. Tables 2 and 3 list the properties of the reinforcing bars and the concrete of each coupling beam specimen used in the analysis, which were derived from test results. Fig. 3 shows a typical finite element mesh used in the analysis. In order to simulate the testing conditions of the coupling beam specimens, the steel loading frame and the rotation restraining mechanism have also been included in the mesh. During the analysis, the load was applied in the form of prescribed displacement at the loading point, which was incremented from zero in steps of 0.2 mm until a maximum value of 60 mm was reached. On the other hand, the reaction force at the loading point was taken as the applied load.

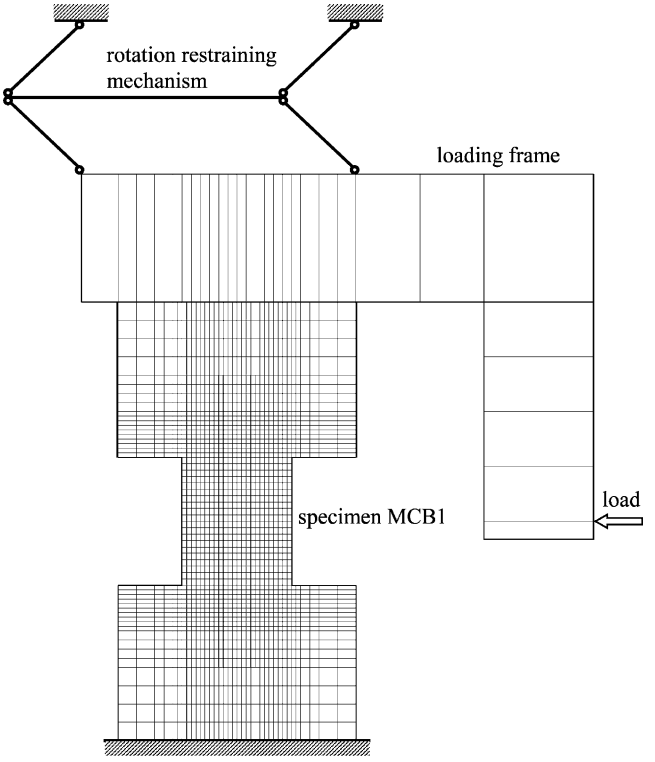


Fig. 3. Finite element mesh used to analyse MCB1.

### 4.1. Load–deflection behaviours

The theoretically evaluated load–deflection curves of the four specimens are presented together with the experimentally measured load–deflection curves in Fig. 4. In Fig. 4, the applied load plotted is the reaction force at the loading point, which corresponded to the load measured by the load cell within the actuator, while the deflection plotted is the lateral displacement of the specimen at the top right corner, which corresponded to the displacement measured by LVDT no. D2 during the test.

The experimental results revealed that the load–deflection curve of MCB1, which failed in shear, has no

Table 3
Properties of the concrete[a]

| Specimen | Age (day) | $f_{cu}$ (MPa) | $f_c$ (MPa) | $\varepsilon_{co}$ ($\mu\varepsilon$) | $f_t$ (MPa) | $\varepsilon_t$ ($\mu\varepsilon$) | Poisson's ratio $\nu$ | $E_o$ (GPa) |
|---|---|---|---|---|---|---|---|---|
| MCB1 | 36 | 55.8 | 37.4 | 3000 | 3.1 | 180 | 0.19 | 24.6 |
| MCB2 | 33 | 56.1 | 37.6 | 3000 | 3.1 | 180 | 0.18 | 23.9 |
| MCB3 | 57 | 48.6 | 32.6 | 3000 | 2.9 | 180 | 0.20 | 23.6 |
| MCB4 | 33 | 49.6 | 33.2 | 3000 | 3.0 | 180 | 0.15 | 24.2 |

[a] $f_{cu}$, $f_c$ and $f_t$ are the cube compressive strength, unconfined uniaxial compressive strength and tensile strength of the concrete. $\varepsilon_{co}$ and $\varepsilon_t$ are the strains at peak compressive stress and at peak tensile stress.

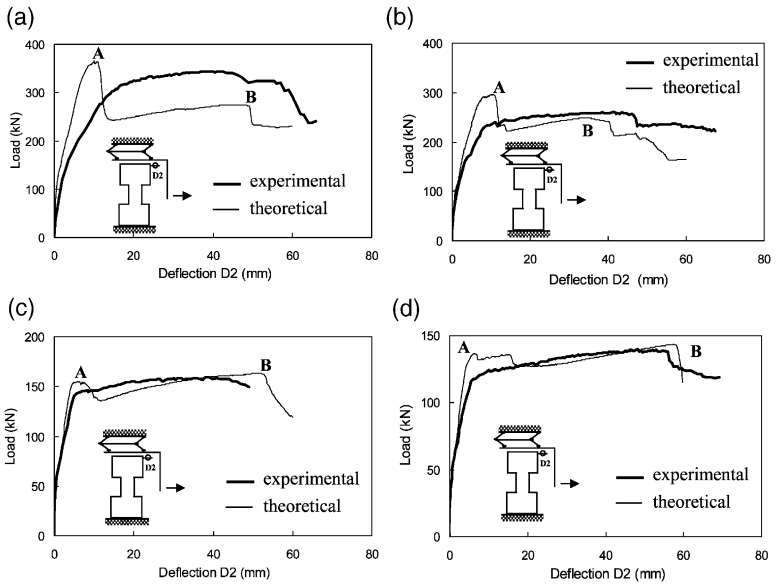


Fig. 4. Theoretical and experimental load–deflection curves of the specimens. (a) MCB1 ($L/H$=1.17); (b) MCB2 ($L/H$=1.40); (c) MCB3 ($L/H$=1.75); (d) MCB4 ($L/H$=2.00).

obvious yield point, while the load–defection curves of MCB2, MCB3 and MCB4, which failed in flexure, have obvious yield points at deflections of around 4–6 mm. On the whole, the theoretical load–deflection curves of the four specimens agree quite well with the corresponding experimental curves. However, whilst the experimental curves are comparatively smooth, each exhibiting a flat yield plateau with no obvious peak points, the theoretical curves are more zigzag, each showing ups and downs after reaching the first peak point. On each theoretical curve in Fig. 4, the first and second peak points are marked as A and B, respectively. It is noteworthy that in each of the specimens MCB1 and MCB2, the load at point A is higher than that at point B, but in each of the specimens MCB3 and MCB4, the load at point A is lower than that at point B.

For comparison, the theoretically evaluated loads and deflections at points A and B are tabulated side by side with the experimentally measured maximum loads and deflections at maximum loads in Table 4. It is seen that the theoretically evaluated maximum loads (in each specimen, the maximum load is taken as the larger value of the load at point A and the load at point B) are in general slightly higher than the experimentally measured maximum loads, the errors being only 5.8%, 13.8%, 3.1% and 2.1% for the specimens MCB1, MCB2, MCB3 and MCB4, respectively. Moreover, for each specimen, the theoretically evaluated deflection at point B agrees quite well with the experimentally measured deflection at maximum load.

However, it is also evident from Fig. 4 that near point A, the theoretically evaluated load–deflection curves do not agree well with the experimentally measured load–deflection curves, especially for the specimens MCB1 and MCB2. In fact, it may be questioned why there should be such a peak point A in each of the theoretically evaluated load–deflection curves whereas no such peak points have been observed in the experiments. A closer look at the numerical results of the theoretical analysis revealed that the discrepancy between the theoretical and

Table 4
Experimental and theoretical peak loads and deflections at peak loads

| Specimen | Experimental | | Theoretical | | | |
|---|---|---|---|---|---|---|
| | At peak load | | At point A | | At point B | |
| | Load (kN) | Deflection (mm) | Load (kN) | Deflection (mm) | Load (kN) | Deflection (mm) |
| MCB1 | 344 | 42.5 | 364 | 10.8 | 274 | 44.2 |
| MCB2 | 260 | 41.0 | 296 | 10.3 | 249 | 35.1 |
| MCB3 | 159 | 38.0 | 155 | 6.2 | 164 | 51.4 |
| MCB4 | 140 | 48.2 | 137 | 6.2 | 143 | 57.4 |

the experimental load–deflection curves near point A is due to the following reasons.

1. In all the specimens, flexural cracks were formed at the tension sides of the beam–wall joints soon after the loads were applied. During the tests, it was observed that once formed, the flexural cracks gradually opened up. Associated with the finite widths of the flexural cracks, bond-slip of the main reinforcing bars there also occurred. The opening up of the flexural cracks and the pullout of the reinforcing bars at the joints contributed significantly to the rotations and thus the lateral deflections of the coupling beam specimens. In the finite element analysis, however, perfect bond of the reinforcing bars was assumed and thus although the cracked elements could have very large tensile strain induced, the smeared cracks could not have finite widths. As a result, the additional deflections of the specimens due to opening up of the flexural cracks and pullout of the reinforcing bars have not been properly modelled. That is why in Fig. 4, the theoretical curves are steeper than the experimental curves after the joints have cracked (within the parts of the curves prior to reaching point A).
2. In the finite element analysis, after the first peak load (point A) was reached, substantial stress redistribution occurred even with very small increment of displacement at the loading point, leading to rapid increase of the tensile strains developed in the cracked elements. As a result, although the stress–strain curve of the concrete under tension has a descending branch, the tensile stresses developed in the cracked elements decreased almost immediately to negligible values after point A was reached. That is why in Fig. 4, the theoretical curves dropped after reaching point A quite rapidly, resulting in fairly sharp peaks at point A, which do not exist in the experimental curves. The root cause of this problem was that in the real structure, the tensile strains in the concrete were highly localised at the cracks and the concrete between two adjacent cracks continued to contribute to the load resistance of the structure by means of tension stiffening, but in the finite element analysis, due to the adoption of the smeared crack model, such strain localization and tension stiffening could not be properly modelled, leading to inaccurate estimation of the effective stiffness of cracked concrete.

The above problems with the finite element method are not easy to resolve. To overcome these problems, further refinement of the finite element method taking into account bond-slip of the reinforcing bars and strain localization of the cracked concrete is needed. Nevertheless, it is still considered that apart from the slight discrepancy between the theoretical and experimental load–deflection curves near point A, the finite element analysis has overall speaking produced theoretical load–deflection curves in good agreement with the experimental results.

### 4.2. Crack patterns and failure modes

The theoretically predicted crack patterns of the four specimens when the lateral deflections corresponded to point B on the load–deflection curves are compared to the experimentally observed crack patterns in Figs. 5 and 6. In the theoretical crack patterns shown, the cracks are drawn as crack marks in the finite elements such that the width and length of each crack mark are proportional to the tensile strain in the direction normal to the crack.

During the tests, it had been observed that in all the specimens, flexural cracks were first formed at the tension sides of the beam–wall joints soon after the loads were applied. As the applied load increased, these flexural cracks extended slightly into the wall panels and then turned to run parallel to the beam–wall interfaces. At the same time, new flexural cracks appeared in the beams at the tension sides of the beams. Upon further loading, many of the flexural cracks formed inside the beams turned to an inclined direction and propagated towards the compression corners at the beam–wall joints to become combined flexural and shear cracks. Eventually, diagonal shear cracks also appeared within the coupling beams. The theoretically predicted crack patterns obtained by the finite element analysis are in good agreement with the observed crack patterns at the various stages of the tests.

Both the experimental and theoretical results indicated that the major cracks governing the failure characteristics of the coupling beam specimens were the flexural cracks formed at the beam–wall interfaces. These flexural cracks propagated from the tension corners of the beam–wall interfaces to the compression corners until they cut through approximately 3/4 of the beam–wall interfaces, leaving behind only about 1/4 of the beam–wall interfaces remaining uncracked. Thus, prior to failure, the compression zones at the beam–wall interfaces had depths of only 1/4 of the respective beam depths. With such small concrete compressive zones effective in resisting shear, there should have been a tendency for the coupling beam specimens, especially those with relatively small span/depth ratios, which were subjected to fairly high nominal shear stresses, to fail by sliding along the beam–wall joints.

Evidently, coupling beams with different span/depth ratios could fail in different failure modes. During the experimental study, the failure modes were determined from the gradual development of crack pattern, opening up of the cracks, yielding of the steel reinforcing bars, crushing of the concrete and deformed shapes of the models after the tests. On the other hand, from the finite element analysis results, the theoretically predicted fail-

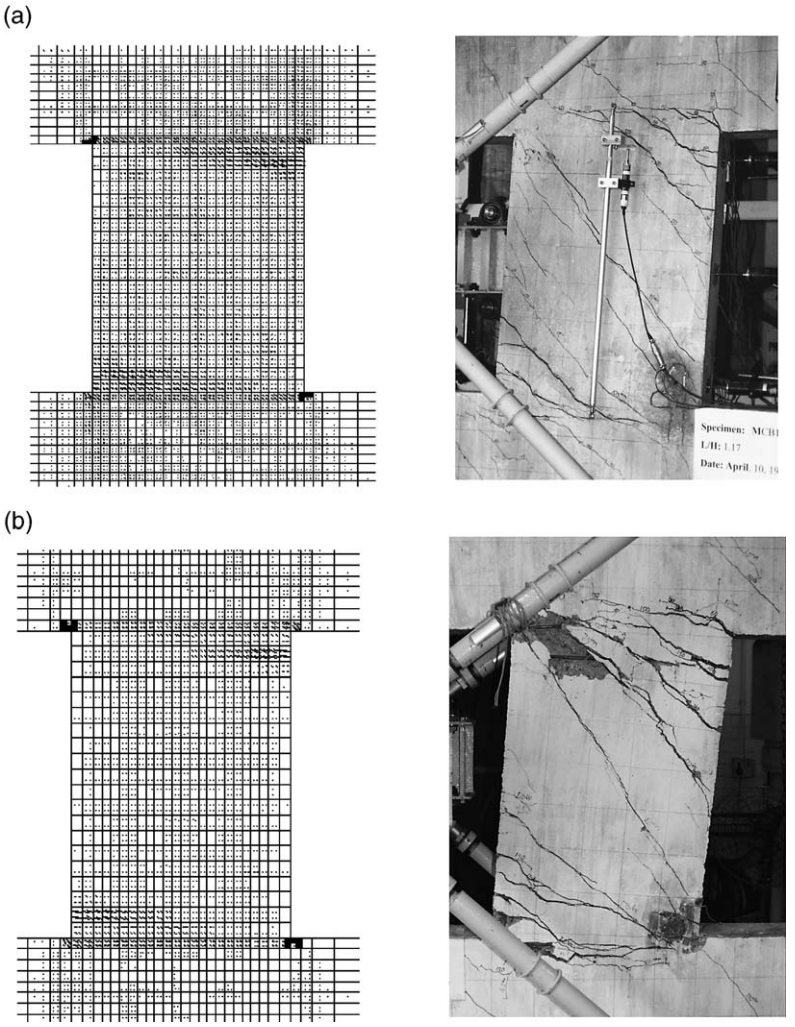


Fig. 5. Predicted and observed crack patterns of MCB1 and MCB2. (a) MCB1; (b) MCB2.

ure modes were determined from the changes in crack pattern with the loading stage as plotted in Figs. 5 and 6, increases in tensile and shear strains of the cracks, yielding of the steel reinforcing bars and crushing of the concrete during failure as revealed from the numerical results. Table 5 presents the experimentally observed and theoretically predicted failure modes of the four coupling beam specimens. The experimental results revealed that the specimen MCB1 failed in a shear-tension mode (i.e., failing by yielding of the shear reinforcement and opening up of the diagonal shear cracks near the centre of the coupling beam), while the specimens MCB2, MCB3 and MCB4 failed in a flexural mode (i.e., failing by flexure at the two ends of each coupling beam). On the other hand, the finite element analysis predicted that the specimen MCB1 should fail in a shear-sliding mode (i.e., failing by shear-sliding along the beam–wall joints), and the specimens MCB2, MCB3 and MCB4 should fail in a flexural mode.

Although the theoretically predicted failure modes for MCB2, MCB3 and MCB4 agree with the experimentally observed failure modes, the predicted failure mode for MCB1 is different from the observed one. It should not be unexpected that deep coupling beams would tend to fail in shear. However, there are two possible shear failure modes, namely: the shear-tension mode and the shear-sliding mode. The actual failure mode that would occur is dependent on which failure mode would lead to a lower failure load. If the failure load of the shear-tension mode was lower than that of the shear-sliding mode, the shear-tension mode would occur; otherwise, the shear-sliding mode would occur instead. If, however, the failure loads of the two shear failure modes were very close to each other, then either failure mode could occur; a slight variation of the yield strength of the shear reinforcement or a small error in the theoretical evaluation of the failure loads could lead to a sudden change of the failure mode but little change in the failure load. In the case of the specimen MCB1, although the theoretically predicted failure mode is different from the observed one, the theoretically evaluated failure load actually differs from the experimentally measured failure

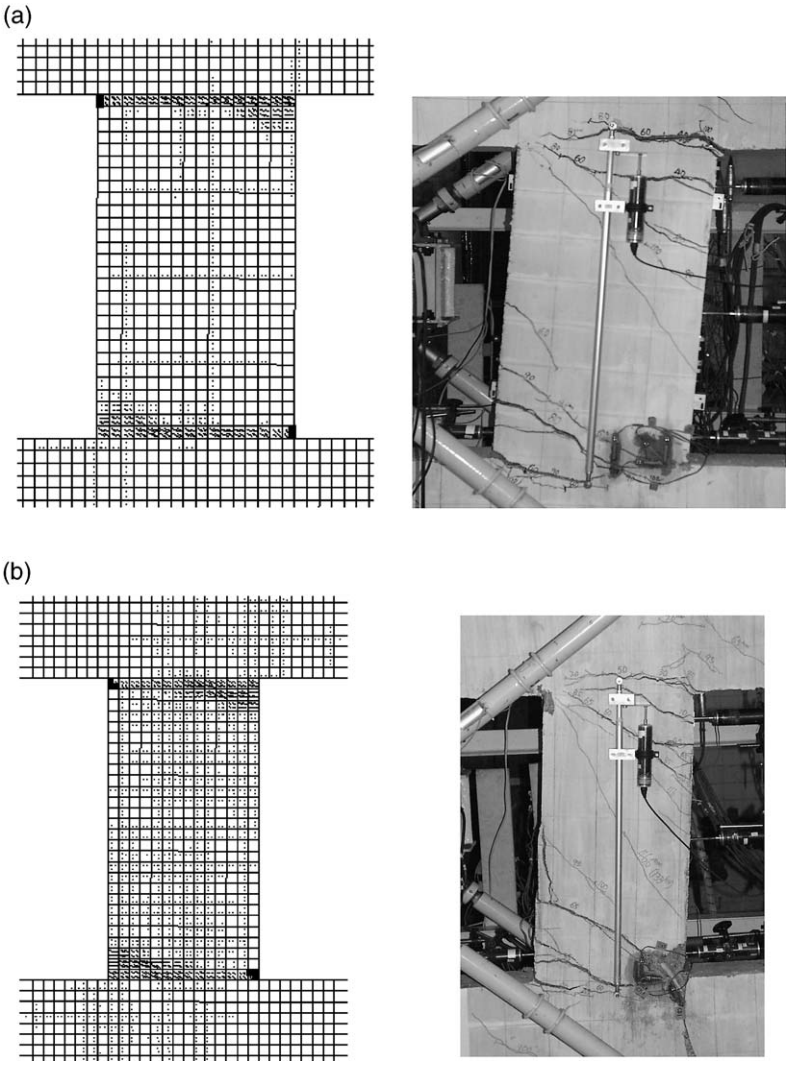


Fig. 6. Predicted and observed crack patterns of MCB3 and MCB4. (a) MCB3; (b) MCB4.

Table 5
Experimentally observed and theoretically predicted failure modes

| Specimen | Experimentally observed | Theoretically predicted |
|---|---|---|
| MCB1 | Shear-tension failure preceded by yielding of shear reinforcement | Shear-sliding failure at beam–wall interfaces |
| MCB2 | Flexural failure | Flexural failure |
| MCB3 | Flexural failure | Flexural failure |
| MCB4 | Flexural failure | Flexural failure |

load by only 5.8%. The probable reason was that the failure loads of the two shear failure modes were actually quite close to each other, as reflected by the close agreement between the theoretically evaluated and the experimentally measured failure loads despite the fact that the theoretical failure mode is different from the observed one.

### *4.3. Axial elongation*

The test results revealed that all the coupling beam specimens elongated significantly in the axial direction when subjected to further loading in the lateral direction after cracking. The theoretical results also indicated that after a certain stage of loading, which matched quite

closely with the time of cracking, the coupling beam specimens would start to elongate. Fig. 7 plots the axial elongation versus the lateral deflection of each of the four specimens, as obtained by experiment and by finite element analysis. It is seen that on the whole the theoretical axial elongation–lateral deflection curves agree quite well with the corresponding experimental curves. However, the theoretical curves are sometimes lower than the experimental curves at large lateral deflections, especially for the specimens MCB1 and MCB2. This implies that the finite element method tends to underestimate the axial elongations of deep coupling beams at large lateral deflections.

Based on the crack patterns shown in Figs. 5 and 6, it is postulated that the mechanism leading to axial elongation of the coupling beams may be described as in the following. After cracks were formed, each coupling beam behaved more like a truss consisting of a diagonal concrete strut under compression and the longitudinal reinforcing bars under tension, as shown in Fig. 8. When the coupling beam was subjected to further shear load, the truss deflected laterally and the diagonal strut rotated about the compressive zones of the beam–wall interfaces. It was the rotation of the strut that led to axial elongation of the coupling beam.

Assuming that the compression zones were of depth equal to 1/4 of the depth of the beam–wall interfaces, the inclination angle $\theta$ of the diagonal strut may be estimated from the equation: $\tan\theta = (4/3)(L/H)$ where $L$ and $H$ are the clear span and depth of the coupling beam. When the diagonal strut rotated by an amount equal to $\Delta\theta$, the corresponding axial elongation $\Delta L$ and lateral deflection $u$ may be evaluated as:

$$\Delta L = 0.75H\Delta\theta + L\varepsilon_c \quad (1)$$

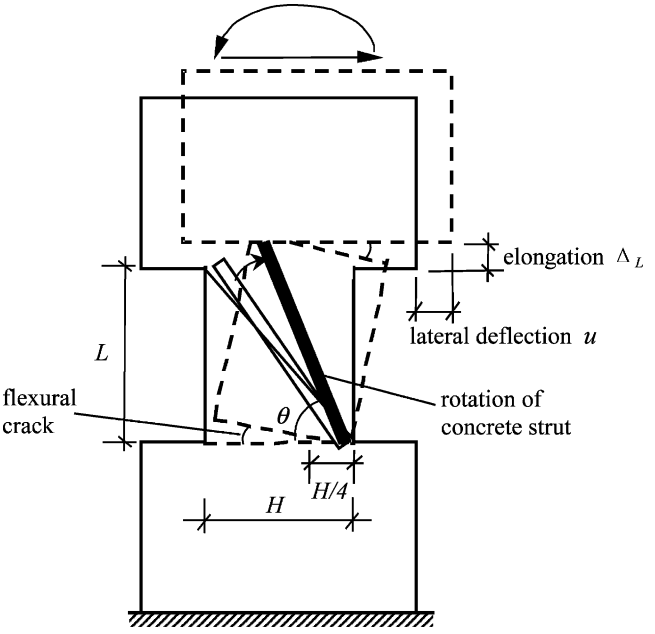


Fig. 8. Mechanism of beam elongation due to concrete strut rotation.

$$u = L\Delta\theta - 0.75H\varepsilon_c \quad (2)$$

in which $\varepsilon_c$ is the strain developed in the diagonal concrete strut. Solving the above equations, the following relation between the axial elongation and the lateral deflection may be obtained:

$$\Delta L = 0.75(H/L)u + (0.56H^2/L + L)\varepsilon_c \quad (3)$$

It has been found from both experimental measurement and finite element analysis that at small lateral deflection, the strain in the concrete strut varied with the lateral deflection, but at large lateral deflection within

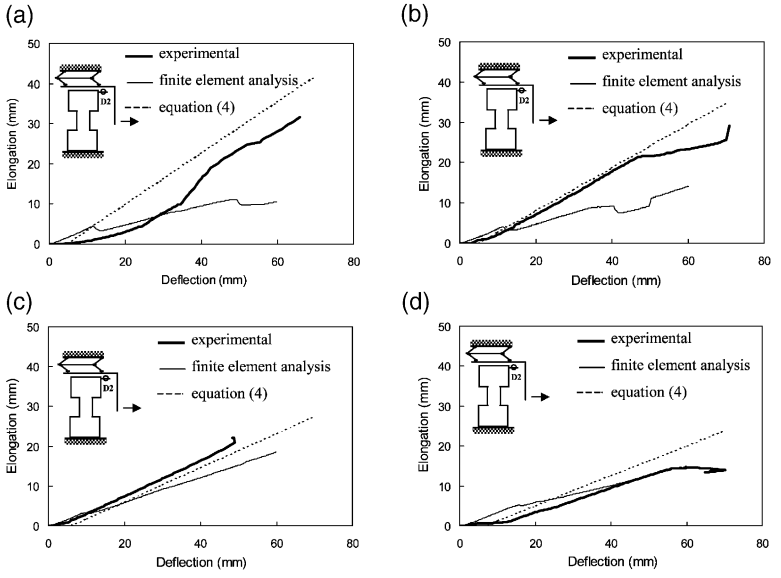


Fig. 7. Axial elongation-lateral deflection curves of the specimens. (a) MCB1 ($L/H$=1.17); (b) MCB2 ($L/H$=1.40); (c) MCB3 ($L/H$=1.75); (d) MCB4 ($L/H$=2.00).

the yield plateau region of the load–deflection curve, the load remained approximately constant and the strain in the concrete strut reached a maximum negative value of about −0.3% (compressive strain is negative). Hence, at large lateral deflection within the yield plateau region, the relation between the axial elongation and the lateral deflection may be simplified as:

$$\Delta L = 0.75(H/L)u - 0.003 \times (0.56H^2/L + L) \quad (4)$$

The above equation is plotted in Fig. 7, from which it can be seen that the equation agrees fairly well with the experimental and finite element analysis results.

The mechanism shown in Fig. 8 may also be used to explain why the finite element method tends to underestimate the axial elongations of deep coupling beams. In the finite element modelling, perfect bond of the reinforcing bars is assumed and thus the flexural cracks at the beam–wall joints cannot really open up as illustrated in Fig. 8. As a result, the rotation of the diagonal concrete strut is hindered to some extent and the finite element model tends to underestimate the rotation angle of the diagonal strut and the axial elongation of the coupling beam.

## 5. Parametric studies

### 5.1. Effect of shear reinforcement

Deep reinforced concrete coupling beams tend to fail in shear, which is a brittle mode of failure. Therefore, when designing deep coupling beams, it is necessary to provide sufficient shear reinforcement to avoid shear failure. However, there are two possible modes of shear failure: shear-tension failure and shear-sliding failure. It is not easy to suppress both modes of shear failure just by adding more shear reinforcement, as will be seen in the following study.

To investigate the effect of shear reinforcement, a parametric study using finite element analysis has been carried out. The specimen MCB1 was selected for the study. Three cases were analysed. In Case 1, the specimen was provided with half the amount of shear reinforcement provided in the model test (R8 @ 150 mm c/c, $\rho_{sv}$ = 0.54%). In Case 2, the specimen was provided with the same amount of shear reinforcement as in the model test (R8 @ 75 mm c/c, $\rho_{sv}$ = 1.07%). In Case 3, the specimen was provided with double the amount of shear reinforcement provided in the model test (R8 @ 37.5 mm c/c, $\rho_{sv}$ = 2.14%). Apart from the shear reinforcement, the other structural parameters were kept the same as those of the real model tested.

Fig. 9 plots the load–deflection curves obtained in the three cases by finite element analysis. In Case 1, with the smallest amount of shear reinforcement provided, the peak load reached was the lowest. In Case 2, with a somewhat larger amount of shear reinforcement provided, the peak load reached was higher but the increase in peak load was not in proportion to the increase in the amount of shear reinforcement. In Case 3, with the largest amount of shear reinforcement provided, the peak load reached has remained basically the same as that reached in Case 2. Hence, when the amount of shear reinforcement increases to beyond certain limit, there is no further increase in shear strength.

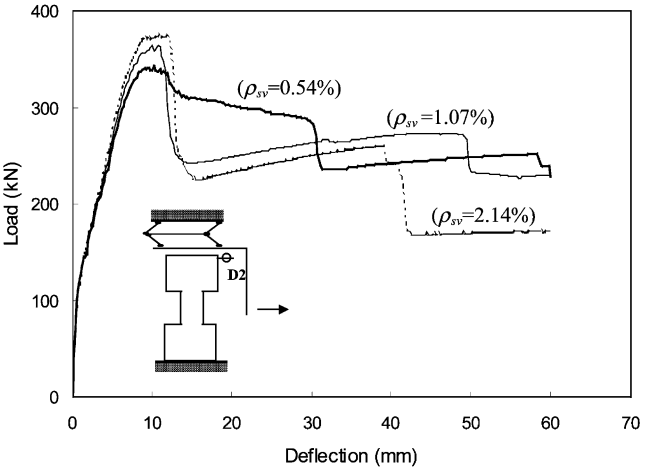


Fig. 9. Effect of varying shear reinforcement in specimen MCB1.

Accompanied with the change in the peak load reached, there appear in Fig. 9 also certain changes in the post-peak behaviour. In Case 1, with the smallest amount of shear reinforcement provided, the load–deflection curve descended at a slower rate after reaching the peak indicating that the specimen failed in a relatively less brittle manner. In Cases 2 and 3, the load–deflection curves descended fairly rapidly at the post-peak stage indicating very brittle failure of the specimen. Detailed study of the finite element results revealed that the difference in post-peak behaviour was due primarily to the different modes of failure. In Case 1, the specimen failed in the shear-tension mode. This mode of failure is characterised by the numerous diagonal cracks formed in the coupling beam, yielding of the shear reinforcement before failure, and opening up of the diagonal cracks until complete failure. In Cases 2 and 3, the specimen failed in the shear-sliding mode. This mode of failure is characterised by the formation of deep flexural cracks at the beam–wall joints, sliding movement along the cracks at the beam–wall joints during failure, and reliance on the dowel action of the longitudinal reinforcing bars at the beam–wall joints for residual shear strength at post-peak stage.

Comparing the numerical results from the three cases analysed, it is evident that the shear-sliding failure mode is more brittle than the shear-tension failure mode, for the obvious reason that the shear-sliding mode is not preceded by yielding of the shear reinforcement whereas

the shear-tension mode is always preceded by yielding of the shear reinforcement. In any case, both modes of shear failure are brittle in nature and should be avoided. However, the addition of more shear reinforcement to suppress shear-tension failure could lead to shear-sliding failure, which is even more dangerous. Hence, during the design of deep coupling beams, sufficient shear reinforcement should be provided to prevent shear-tension failure but care should be taken to avoid putting in excessive shear reinforcement, which could trigger shear-sliding failure.

### 5.2. Effect of restraint against axial elongation

In the model testing and the finite element analysis simulating the model tests, the boundary conditions were applied in such a way that the coupling beam specimens were free to elongate in the axial direction without any restraint. However, in a real coupled shear wall structure, the coupling beams are not necessarily free to elongate. First, if there are floor slabs connected to the coupling beams, the in-plane stiffness of the floor slab would act as restraint against the axial elongation of the coupling beams. Second, even if there are no floor slabs connected to the coupling beams, the lateral stiffness of the walls could to some extent restrain the axial elongation of the coupling beams. Any such restraint against the axial elongation of the coupling beams would impose axial compression loads onto the coupling beams and change the nonlinear behaviour of the coupling beams.

In order to investigate the effect of any restraint against axial elongation on the nonlinear behaviour of deep coupling beams, the specimen MCB1 has been re-analysed by the finite element method with the displacement boundary conditions applied such that the axial elongation of the coupling beam was fully restrained. Fig. 10 presents the load–deflection curves of MCB1 obtained with or without the restraint against axial elongation applied. It can be seen from the figure that the load–deflection curve of the coupling beam changed quite substantially when restraint against axial elongation was applied. With axial elongation fully restrained, the coupling beam was able to withstand substantially higher lateral load but it also failed in a more brittle manner. Detailed study of the finite element analysis results revealed that the restraint against axial elongation had induced fairly high compressive stresses onto the diagonal concrete strut formed inside the coupling beam and caused the coupling beam to fail in shear by crushing of the diagonal concrete strut (this mode of failure may be described as shear-compression mode). Hence, it may be concluded that any restraint against axial elongation could significantly affect the nonlinear behaviour of deep coupling beams and should thus be properly simulated or allowed for in model testing and theoretical analysis. Further study on the effect of restraint against axial elongation is recommended.

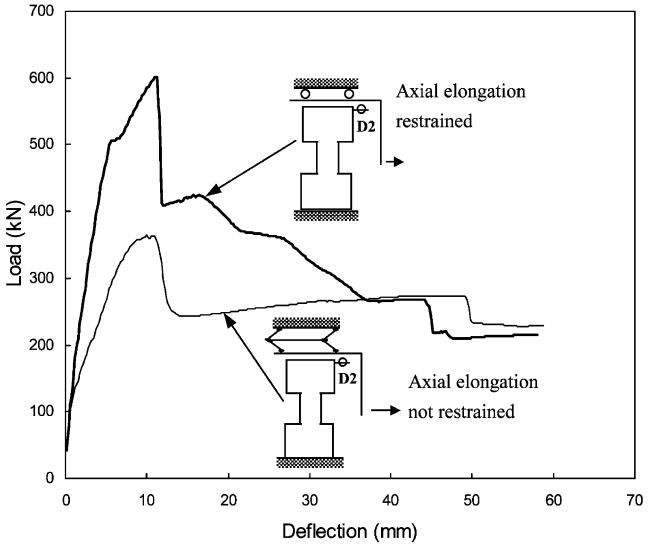


Fig. 10. Effect of restraining axial elongation of specimen MCB1.

## 6. Conclusions

The nonlinear behaviour and failure characteristics of deep reinforced concrete coupling beams under monotonic loading condition have been studied by applying the nonlinear finite element method recently developed by the second and third authors to analyse the large scale coupling beam models previously tested by the first and second authors. Comparison of the finite element analysis results to the experimental results showed good agreement in the load–deflection curves, maximum loads, crack patterns, failure modes and axial elongations, except minor discrepancies due to inadequate modelling of the bond-slip of reinforcing bars and the strain localization of cracked concrete. On the whole, the finite element method is capable of dealing with deep reinforced concrete coupling beams, but further refinement taking into account bond-slip of reinforcing bars and strain localization and tension stiffening of cracked concrete is recommended.

Based on the previous experimental results and the details revealed by the present finite element analysis, it may be concluded that the flexural cracks formed at the tension sides of the beam–wall joints and the diagonal shear cracks formed near the centre would together govern the nonlinear behaviour and failure characteristics of a coupling beam. The flexural cracks at the beam–wall joints would, once formed, gradually open up leading to significant local rotations at the joints and propagate to the compression sides of the joints until only 1/4 of the beam depth remain uncracked causing small effective concrete area for resisting shear and high tendency to fail by shear-sliding. On the other hand, after formation of the diagonal shear cracks, the coupling beam behaves

more like a truss consisting of a diagonal concrete strut and the longitudinal reinforcing bars. The transverse component of the compression developed in the diagonal strut acts against the applied shear load while the longitudinal component pushes the two walls at the ends apart. As the coupling beam deflects laterally, the diagonal strut rotates resulting in axial elongation of the coupling beam. A structural model is yet to be developed, but one thing for sure is that deep coupling beams behave very differently from ordinary beams and should not be modelled as beams.

Lastly, parametric studies on the effects of varying the shear reinforcement and restraining the axial elongation of the coupling beams have been carried out. It was found that although adding more shear reinforcement could increase shear strength and suppress shear-tension failure, it would also lead to shear-sliding failure, which is even more brittle. It was also found that any restraint against the axial elongation could significantly affect the nonlinear behaviour of deep coupling beams and should thus be properly simulated or allowed for in model testing and theoretical analysis.

## Acknowledgements

The financial support from the Research Grants Council of Hong Kong (Project Ref: HKU 7005/00E) for the research presented herein is gratefully acknowledged.

## References

[1] Paulay T, Priestley MJN. Seismic design of reinforced concrete and masonry buildings. New York: Wiley, 1992.
[2] Kwan AKH, Zhao ZZ.'Reinforced concrete coupling beams: their differences from ordinary beams. In: Proceedings of 7th International Conference on Enhancement and Promotion of Computational Methods in Engineering and Science EPMESC VII, Macao; 1999, vol.1. pp. 581–8.
[3] Tassios TP, Moretti M, Bezas A. On the behavior and ductility of R.C. coupling beams of shear walls. ACI Struct J 1996;93(6):711–20.
[4] Galano L, Vignoli A. Seismic behavior of short coupling beams with different reinforcement layouts. ACI Struct J 2000;97(6):876–85.
[5] Aktan AE, Bertero VV. Seismic response of r/c frame-wall structures. J Struct Engng, ASCE 1984;110(8):1803–21.
[6] Aristizabal-Ochoa JD. Seismic behavior of slender coupled wall systems. J Struct Engng, ASCE 1987;113(1):2221–34.
[7] Glück J. Elasto-plastic analysis of coupled shear walls. J Struct Div, ASCE 1973;99(ST8):1743–60.
[8] Nayar K, Coull AE. lastoplastic analysis of coupled shear walls. J Struct Div, ASCE 1976;102(ST9):1845–60.
[9] Pala S, Özmen G. Effective stiffness of coupling beams in structural walls. Comput Struct 1995;54(5):925–31.
[10] Harries KA, Mitchell D, Redwood RG, Cook WD. Nonlinear seismic response prediction of walls coupled with steel and concrete beams. Can J Civil Engng 1998;25(5):803–18.
[11] Kim HS, Hong SM. Formulation of transition elements for the analysis of coupled wall structures. Comput Struct 1995;57(2):333–44.
[12] Subedi NK. RC-coupled shear wall structures I: analysis of coupling beams. J Struct Engng, ASCE 1991;117(3):667–80.
[13] Subedi NK. RC-coupled shear wall structures II: ultimate strength calculations. J Struct Engng, ASCE 1991;117(3):681–98.
[14] Isenberg J, editor. Finite element analysis of reinforced concrete structures II. New York: ASCE; 1993.
[15] Kotsovos MD, Pavlović MN. Structural concrete: finite element analysis for limit-state design. London: Thomas Telford, 1995.
[16] He XG, Kwan AKH. Modeling dowel action of reinforcement bars for finite element analysis of concrete structures. Comput Struct 2001;79(6):595–604.
[17] Kwan AKH, He XG. Finite element analysis of effect of concrete confinement on behaviour of shear walls. Comput Struct 2001;79(19):1799–810.
[18] Kwan AKH, Zhao ZZ. Testing of coupling beams with equal end rotations maintained and local joint deformation allowed. Proc ICE Struct Build 2002;152(1):67–78.
[19] Kwan AKH, Zhao ZZ. Cyclic behaviour of deep reinforced concrete coupling beams. Proc ICE Struct Build 2002;152(3):283–93.